Article:
Almutairi, F. orcid.org/0009-0001-3168-6776, Alotaibi, M. orcid.org/0000-0003-1322-6992 and West, A.R. orcid.org/0000-0002-5492-2102 (2024) Flash luminescence, resistive switching and metal-insulator transitions in ceramic oxides. Acta Materialia, 276. 120003. ISSN 1359-6454

https://doi.org/10.1016/j.actamat.2024.120003

Acta Materialia 276 (2024) 120003

Contents lists available at ScienceDirect

Acta Materialia

journal homepage: www.elsevier.com/locate/actamat

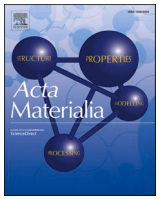

Full length article

Flash luminescence, resistive switching and metal-insulator transitions in ceramic oxides

Fawaz Almutairi [a], Meshari Alotaibi [b], Anthony R West [c,*]

[a] Physics Department, College of Science, Imam Mohammad Ibn Saud Islamic University (IMSIU), Riyadh 13318, Saudi Arabia
[b] Department of Chemistry, College of Science, Taif University, Taif 21944, Saudi Arabia
[c] University of Sheffield, Department of Materials Science & Engineering, Sheffield S13JD, UK

ARTICLE INFO

Keywords:
Resistive switching
Flash luminescence
Oxide ion conductivity
Metal-insulator transition
Yttria-doped hafnia
Bismuth ferrite conductivity

ABSTRACT

A combination of voltage-induced, reversible OFF-ON resistive switching and electroluminescence is reported in two materials that are both mixed conductors of oxide ions and electron holes. This occurs at high temperatures, 450–700 °C in cubic, fluorite-structured hafnia, $Y_xHf_{1-x}O_{2-x/2}$ and at more modest temperatures, 200–300 °C in Ca-doped $BiFeO_3$ with a cubic perovskite structure. In both cases, a small voltage in the range 2–40 V is applied across mm-thick ceramic samples. Both effects are influenced greatly by oxygen exchange with the surrounding atmosphere and involve a combination of electron injection at the cathode, hole injection at the anode and generation of internal *pn* junctions. There are strong similarities between these effects and flash sintering but without the significant sintering, thermoluminescence and Joule heating that may be observed with flash sintering.

1. Introduction

In this paper, we report a clear link between two separate phenomena in bulk oxide materials, voltage-induced luminescence and a metal-insulator transition that is responsible for reversible resistive switching. Luminescence associated with flash sintering has become of much interest in recent years as flash sintering represents a novel, economic method to sinter materials, especially, but not exclusively, ceramic oxides [1,2]. Flash sintering was first demonstrated in the oxide ion conductor yttria-stabilised zirconia (YSZ). It involved preparation of a dog-bone shaped powder compact and application of a small voltage, typically 100 V/cm via Pt leads, to the ends of the dog bone. The temperature was gradually increased from a starting temperature of typically 900 °C [3]. A small increase in conductivity occurred during a premonitory period, until the flash event which had three characteristic features: a sharp increase in conductivity, rapid sintering of the sample in a few seconds and luminescence; hence the name flash sintering for this phenomenon [1-4]. Since then, many studies have reported its applicability as a rapid sintering technique for a wide range of materials; work has continued to understand the mechanisms responsible for the different aspects [2,5] but the phenomenon is still not well-understood.

Reversible resistive switching occurs in two characteristic sets of materials. First, in transition metal-containing bulk materials, it is usually associated with a temperature-induced crystallographic phase transition, such as the Verwey transition in magnetite, Fe_3O_4 and oxides such as VO_2 [6-10]. Structural changes at the phase transition impact on the electronic conductivity which involves localised hopping in the insulating OFF state that switches to band type, delocalised conduction in the metallic ON state. This may also be described as a Mott transition in which the localised electrons, or small polarons, in the OFF state become large polarons in the ON state [9,11-13].

Second, in nanometre-thick materials, resistive switching can be voltage-induced and this has led to the development of memristors for possible memory applications [14-16]. Different types of switching have been identified as either volatile or non-volatile depending on whether a reverse bias is required to switch back to the OFF state. Within the non-volatile group, the mechanism may be unipolar or bipolar depending on the polarity of the bias required to switch to the OFF state. A widely-observed feature of memristive switching is the formation of conductive filaments during a preliminary forming stage [14-16]. These subsequently break and reform repeatedly as the main switching mechanism. A third possibility, threshold switching, involves the creation / annihilation of carriers in a cascade effect.

In bulk materials, reversible resistive switching induced by a small

* Corresponding author.
E-mail address: a.r.west@sheffield.ac.uk (A.R. West).

https://doi.org/10.1016/j.actamat.2024.120003
Received 8 January 2024; Received in revised form 8 April 2024; Accepted 11 May 2024
Available online 14 May 2024

voltage in the range 1–30 V that does not involve a phase transition has been demonstrated as a new phenomenon in two groups of materials: first, Ca-doped bismuth ferrite (BCF), $Bi_{1-x}Ca_xFeO_{3-\delta}$ [17] which has a cubic perovskite structure; second, yttria-stabilised hafnia (YSH), $Y_xHf_{1-x}O_{2-x/2}$, [18] which is isostructural with well-studied YSZ analogues and has a cubic defect fluorite structure. In both cases, a *dc* bias voltage was applied at the same time as *ac* impedance measurements were made. Initially, the electronic conductivity increased gradually until a rapid increase in conductivity by 2–4 orders of magnitude caused an OFF-ON transition. The conductivity increase was reversible, with some hysteresis, on removal of the bias. In the BCF case, the conductivity increase was shown to be isotropic and not filamentary. Impedance measurements showed that in both cases, the sample-electrode arrangements did not contain a significant Schottky barrier contribution to the overall impedance; instead, the impedance was dominated by the sample bulk, which included a possible grain boundary contribution [17].

Voltage-induced resistive switching of bulk ceramics is clearly different from both memristive switching of thin films and flash sintering. With BCF, the applied voltage (1–30 V) is small, the temperature is low (25–120 °C) and the samples do not sinter. The switching occurs in mm-thick samples which are about 6 orders of magnitude thicker than nm-thick films in typical memristors [3,19], but the magnitude of the applied voltage is similar or only slightly greater. Although extensive studies of flash sintering have been reported, its three characteristic features, referred to above, are not always observed. Thus, a flash event has been observed in YSZ single crystals without any evidence of microstructural changes or sintering. Certainly, there is a dramatic increase in both conductivity and temperature during flash sintering, but there is still debate about whether Joule heating is partially or wholly responsible for the phenomenon. The observed reversible resistive switching in BCF and YSH occurs under mild conditions of voltage and temperature and appears to be separate from flash sintering which requires more extreme conditions.

The luminescence in flash sintering is usually attributed to thermoluminescence. Here, we demonstrate that, under certain circumstances, the observed reversible OFF-ON resistive switching in BCF and YSH is accompanied by reversible OFF-ON switching of luminescence but without evidence of significant sintering. The temperature changes during switching are limited to a few degrees and the luminescence must be electro- rather than thermo- in origin.

2. Experimental procedure

YSH15 ($Hf_{0.85}Y_{0.15}O_{1.925}$) and BCF23 ($Bi_{0.77}Ca_{0.23}FeO_{3-\delta}$) were prepared by high temperature solid state synthesis. YSH15 powders were prepared by reacting HfO_2 and Y_2O_3 in air in an Al_2O_3 crucible at 1300 °C for 10 h, ground, pressed into pellets and sintered at 1750 °C for 16 h, as described previously [20]. BCF23 was synthesised using Bi_2O_3 (99.999 % pure, Acros chemicals), $CaCO_3$ (99 % pure, Sigma-Aldrich) and Fe_2O_3 (99 % pure, Sigma-Aldrich) which were pre-dried at 180, 180 and 400 °C, respectively before weighing. The powders were ground together, pressed into pellets and reaction-sintered in air at 945 °C for 2 h. Phase analysis, using a Bruker D2 Phaser X-ray diffractometer, Cu Kα radiation ($\lambda = 1.5418$ Å), showed that, as expected both samples gave the desired single phase products, Fig. S1; YSZ15 had a cubic fluorite structure and BCF23 had a cubic perovskite structure.

For impedance spectroscopy (IS) measurements, Au paste electrodes were coated on opposite pellet faces, fired at 850 °C for 2 h and then placed between metal electrodes in a conductivity jig inside a tube furnace. For YSH15, IS measurements were performed using an Agilent 4249A Precision Impedance Analyser, frequency range 40 Hz-1 MHz, at the same time as a *dc* voltage was applied. Impedance data were corrected for overall sample geometry and blank permittivity of the jigs; resistance and capacitance values are reported in resistivity and permittivity units of Ωcm and Fcm^{-1}. Similar measurements were made on BCF23 pellets which were reheated at 945 °C and slow cooled in either air or N_2 atmospheres.

Electric fields of typically 145 Vcm^{-1} (YSH) and 198 Vcm^{-1} (BCF) were applied for varying time schedules and the current limit set at ~61 $mAmm^{-2}$. Flashed samples were either quenched by removing from the furnace and cutting off the power supply at the same time, to allow samples to cool rapidly, or cooled in the furnace with the bias applied. For visual observation of flash, experiments were conducted in a furnace fitted with a viewing port. Using a digital camera, light emission from the sample was recorded but luminescence spectra were not recorded. For some experiments, a thermocouple in close proximity to the sample was used to monitor any temperature changes associated with either *dc* bias application or change in pO_2.

3. Results

3.1. Yttria-stabilised hafnia (YSH15)

Typical impedance data for YSH15 are shown in references [18,20] and Fig. S2(a). They show the presence of three main components, attributed with decreasing frequency to bulk, grain boundary and sample-electrode interface impedances. This assignment was determined by reprocessing the same data as capacitance, C' spectroscopic plots on logarithmic scales; these show limiting high, an intermediate and limiting low frequency plateaux of approximate values 2 $pFcm^{-1}$, 100 $pFcm^{-1}$ and 300 μFcm^{-1}, respectively, Fig. S2(c). The high value of the sample-electrode interface capacitance is taken as a signature that oxide ion conductivity is the main conduction mechanism [18,20].

Arrhenius plots, Fig. 1, show the total conductivities of YSH15 measured under three conditions: in air on heating without a *dc* bias; in air and N_2 on heating with 145 Vcm^{-1} *dc* bias; on cooling in air after removal of the bias. Before applying the bias in air, the Arrhenius plot was linear with activation energy 1.19(1) eV; similar data (not shown) were observed in N_2 and O_2. At lower temperatures with an applied bias, the conductivity increased slightly and was higher in air than in N_2, Fig. 1(a,b). This indicates the onset of p-type behaviour, consistent with previous studies on hole creation, Eq. (1), associated with O_2 absorption, redox reaction with lattice oxide ions, O_O^x and subsequent hole location on lattice oxygens, $O_O^\bullet$:

$$V_O^{\bullet\bullet} + O_O^x + 1/2O_2 = 2O_O^\bullet \quad (1)$$

In the absence of a *dc* bias, Eq. (1) is driven slightly to the right in atmospheres of increasing pO_2. With a small applied bias at lower temperatures, Eq. (1) is also driven to the right but to a greater degree, especially in air. Reaction (1) is believed to occur preferentially at the positive electrode (anode) because mobile lattice oxide ions, especially those adjacent to oxygen vacancies near the anode interface, undergo single step ionisation and transfer electrons to incoming absorbed oxygen molecules which dissociate, become singly charged and occupy the vacancies. Effectively, each reaction with $1/2O_2$ is redox in character and leads to the creation of holes on two oxygens which may also be regarded as O^- ions. Consequently, the material becomes a mixed conductor of oxide ions and electron holes.

At higher temperature with continued applied bias, the conductivity increased sharply by ~ three orders of magnitude at~ 450 °C. This was accompanied by a small increase in temperature (~ 8 °C) and the switch to a low activation energy ON state which was maintained up to at least 700 °C (a). At the same time as the OFF-ON conductivity transition, the sample started to luminesce. This was maintained while the conductivity was in the ON state, (d,e), but did not occur in the OFF state before switching (c). In the ON state, the conductivity was higher in N_2 which indicates release of electrons by loss of oxygen from the sample:

$$O_o^x = 1/2O_2 + 2e' + V_o^{\cdot\cdot} \quad (2)$$

This may have commenced during the OFF-ON transition, but

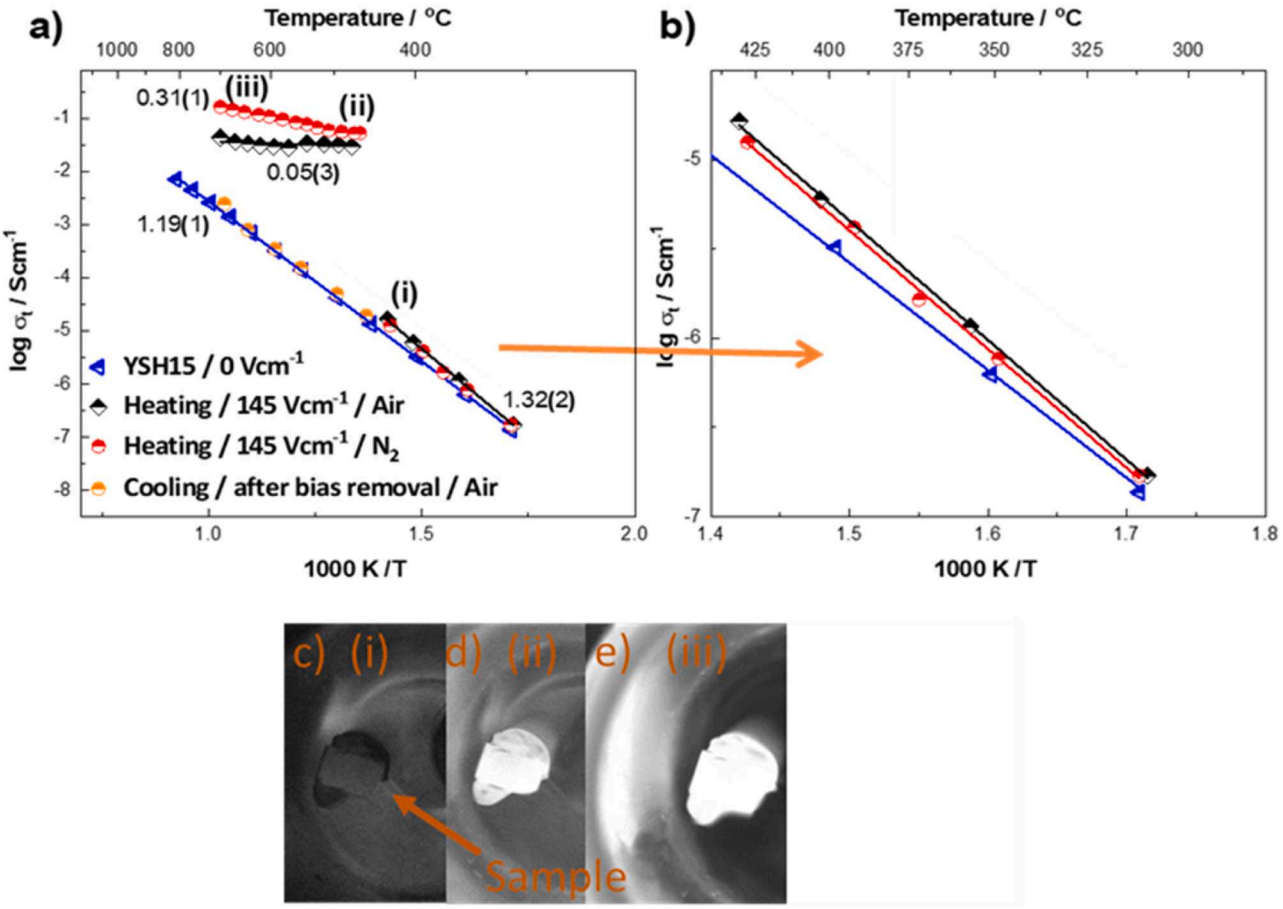

Fig. 1. (a,b) Arrhenius plots of the total conductivity of YSH15: on heating in air without bias; on heating in air and N_2 with bias applied; on cooling in air, bias removed. (c-e) Photographs of the sample (i) before switching, lower conductive state and (ii,iii) after switching, high conductive state at 435 and 700 °C; sample size typically 2 mm thick and 6 mm diameter; see Fig 6(a) for a close-up of pellet and electrode wire coils.

certainly continued at higher temperatures and therefore, indicates a change of mechanism for the electronically conducting component in the ON state from *p*-type to *n*-type. This change of mechanism occurred in parallel with the existence of oxide ion conduction which is the main conduction mechanism in the absence of an applied field. The magnitude of oxide ion conductivity is not expected to change as a consequence of small applied fields as these are unlikely to modify either the activation energy for ion hopping or the number of oxide ion vacancies, but clearly, dramatic changes do occur in the magnitude of electronic conduction.

Eq. (1) involves the single step ionisation of lattice oxide, O^{2-} ions by reaction with O_2 gas. The O_2 molecules dissociate; each O atom picks up only one electron from a lattice oxide ion and occupies a vacant lattice site. This may therefore be regarded as the creation of two O^- ions or alternatively, as holes on two lattice oxygens. A more familiar gas-solid reaction is the double ionisation of lattice O^{2-} ions leading to the liberation of O_2 gas, Eq. (2) and release of electrons into the sample as *n*-type carriers. There are, therefore, two stages in ionisation of lattice O^{2-} ions which may be summarised ideally, as:

$$O_o^x = O_o^{\cdot} + e' \quad (3)$$

$$O_o^{\cdot} = 1/2O_2 + e' \quad (4)$$

These stages may occur separately or be combined into a single step reaction. The first step (3) gives *p*-type carriers, ie O^- ions, assuming that the liberated electrons are trapped, as in Eq. (1); the second step (4) gives *n*-type carriers. Depending on the materials under study and experimental conditions, either single or double ionisation of lattice O^{2-} ions may predominate or both may occur to varying degrees [21]. Results in Fig. 1(a,b) indicate that single ionisation, Eq. (1), occurs under bias at lower temperatures whereas double ionisation (2) dominates in the ON state under the same bias but at higher temperatures.

At the end of the heating cycles with the samples in the ON state, the *dc* bias was removed and impedance data recorded at a few temperatures on cooling. The samples no longer luminesced and the conductivity data were very similar to those on heating without a bias, as shown in Fig. 1(a) for the sample cooled in air. This shows that the bias-induced changes on heating were reversible on removing the bias before cooling.

On cooling with the bias still applied, however, the results were very different, as shown in Fig 2(a) for the sample cooled under bias in either N_2 or air; for comparison, data are also shown for cooling without a bias. The conductivity maintained the ON state with almost zero activation energy, especially in air. The luminescence declined a little in intensity in air at 250 and 100 °C, (b-e), but disappeared completely in N_2 at these temperatures, (f-j).

These results indicate that the occurrence of luminescence has a strong relationship with pO_2 in the surrounding atmosphere and is only, but not always, observed in the ON state. The ON state conductivity is higher in N_2 than in air which is consistent with a greater O_2 loss in N_2 and yet the luminescence is maintained better in air. Since the ON state conductivities are primarily *n*-type, it appears that the presence of O_2 in the atmosphere must lead to formation of a *p*-type region by means of Eq. (1), leading to creation of a *pn* junction between the two carrier-doping regions. Electron-hole recombination, giving luminescence, occurs on passing a *dc* current across the *pn* junction. The holes may be located on oxygen, as in Eq. (1), or on other redox-active species,

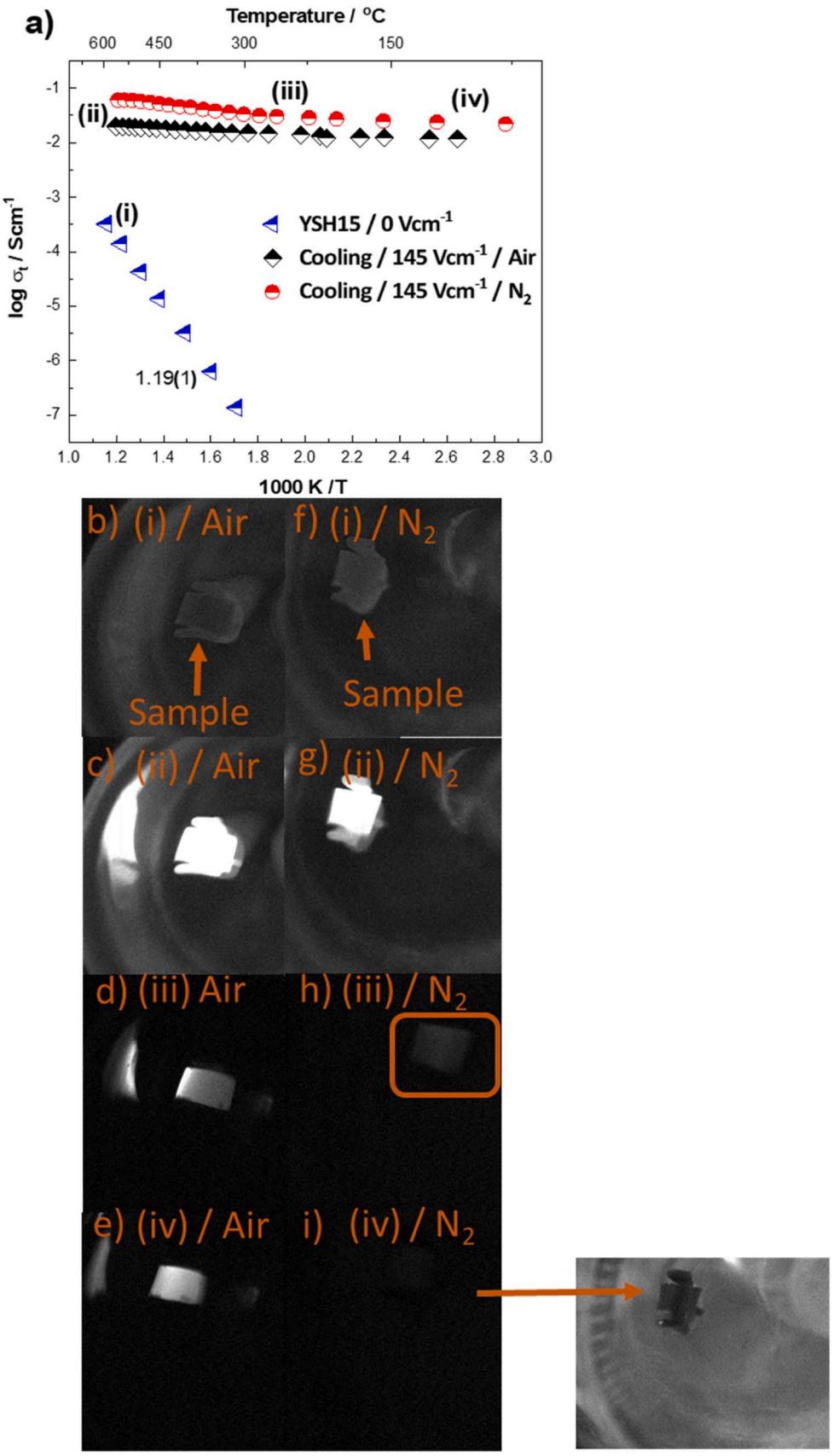

Fig. 2. (a) Arrhenius plots of the total conductivity of YSH15 on cooling under bias in dry air, N_2 and without bias in air. (b,f) Sample photos taken in the OFF state before bias application. (c,d,e) Photos taken during cooling under bias in air at points (ii), (iii) and (iv), diagram (a). (g,h,i) Photos similar to (c,d,e) but taken in N_2, during cooling under bias.

especially Fe^{3+}in BCF (see later); in YSH, there are no possible species for location of the holes other than on oxygen. Logically, under a *dc* bias, hole injection occurs at the anode whereas charge injection of *n*-type carriers occurs at the cathode [17,18,20,21].

Typical impedance data at 495 °C are shown in Fig 3 without (a), with (b) and after removal (a) of 145 V/cm. Without a bias, (a), two semicircles and a small spike are seen which correlate with bulk, grain boundary and the sample-electrode interface impedances. The resistances are slightly less after removal of the bias which may reflect some residual effect of the bias or a small temperature difference. However, during application of the bias (b), the impedance complex plane shows just a small capacitive spike with total resistivity of 32 Ωcm, that is three orders of magnitude lower than the initial resistivity ~ 20 kΩcm and indicates the clear difference, with and without *dc* bias, at essentially the same temperature. On removal of the bias, the sample recovered almost its original state with the same three main components (a), as also shown in the conductivity Y' and capacitance C' presentations of the same data (c, d).

3.2. *Ca-doped bismuth ferrite $Bi_{0.77}Ca_{0.23}FeO_{3-\delta}$ (BCF23)*

Two samples of BCF23 were sintered then slow cooled in different atmospheres, air and N_2. Typical impedance data of both are shown in Figure S3 and are similar to those reported previously [22]. For the air-processed sample, Z* data (a) are dominated by the bulk with no evidence for the presence of other components such as a sample-electrode interface; the C′ spectroscopic plot (b) shows a limiting high frequency plateau of ~10 $pFcm^{-1}$ over most of the frequency range. The absence of a blocking capacitance is good evidence that conduction is primarily electronic, as reported for similarly-prepared materials [22]; conduction is *p*-type because of the dissociation and ionisation process shown in Eq. (1).

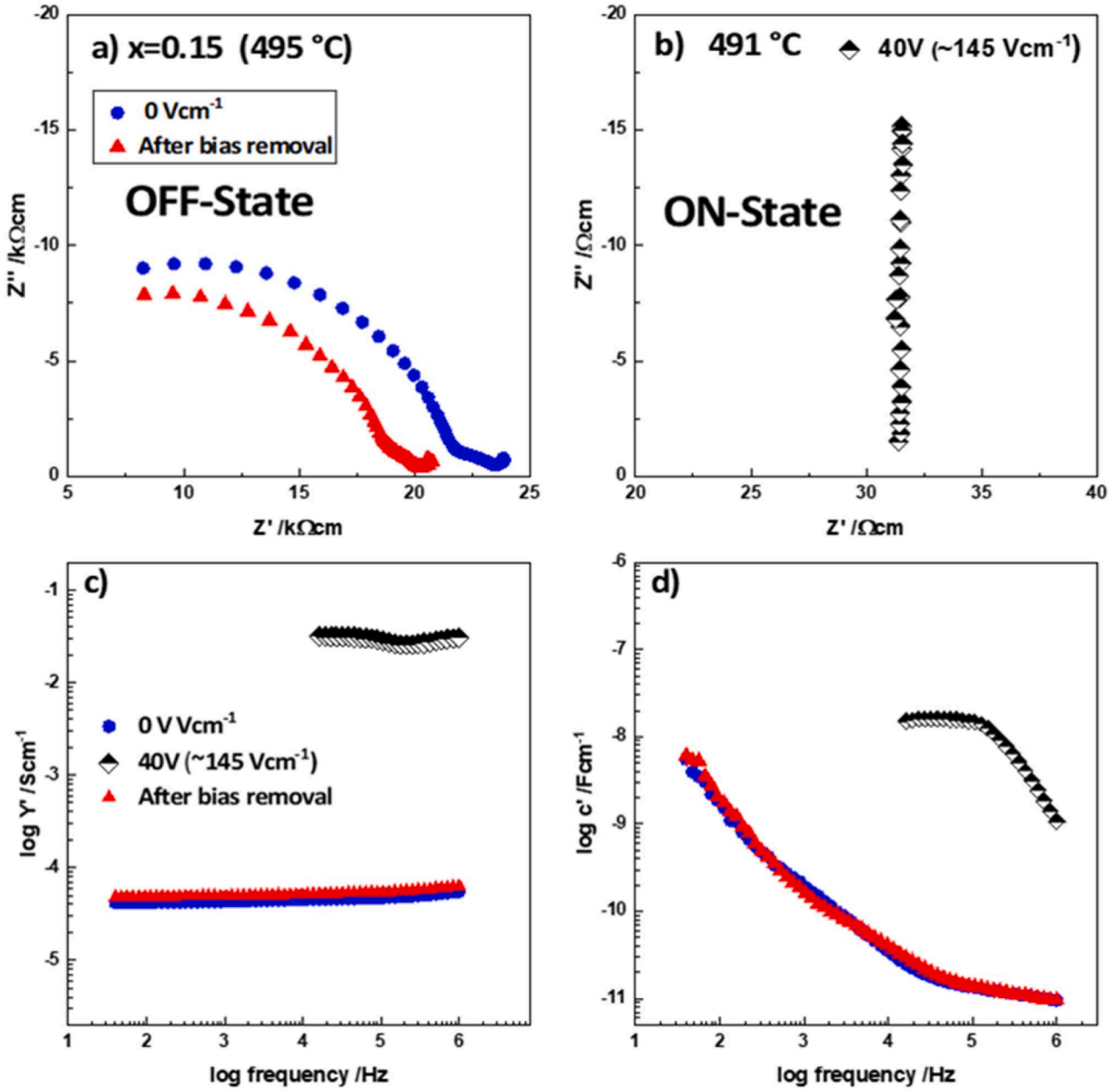

Fig. 3. (a,b) Impedance complex plane plots and c, d) spectroscopic plots of admittance, Y' and capacitance, C' of YSH15 before, during and after bias application / removal.

For the N_2-processed sample, Z* data (c) are again dominated by the bulk but also show a low frequency Warburg spike. The C′ spectroscopic plots (d) show a high frequency bulk capacitance,~ 2×10^{-11} F/cm at 288 °C. At lower frequencies, the value of C′ increased significantly to reach 3×10^{-4} F/cm at 10^{-2} Hz which is characteristic of ion blocking at a sample-electrode interface and double layer phenomena. The presence of a Warburg spike at low frequency, that presumably represents diffusion of oxygen molecules towards, or away from, the sample electrode-interfaces, and the associated high capacitance values are evidence of oxide-ion conduction. The electrical properties of BCF23 are therefore very dependent on processing atmosphere and range from *p*-type electronic to oxide ion conduction.

Arrhenius plots, Fig. 4, show the total conductivities of both samples before and during application of the small *dc* bias. Conductivity of the N_2-processed sample without bias (red data points) was several orders of magnitude lower than that of the air-processed sample and had higher activation energy, 0.72(4) *cf* 0.62(1) eV. It was reported previously that, with decreasing pO_2 during sample preparation and measurement, the conductivity of BCF materials decreased by several orders of magnitude and changed from essentially *p*-type semi-conduction to oxide-ion conduction [22], similar to the results presented here. BCF23 is therefore a good oxide ion conductor but additionally shows *p*-type conductivity with increasing pO_2 and effectively, it becomes a mixed conductor.

On application of a small dc bias and after sufficient equilibration time (black data points), the conductivity of both samples increased dramatically by several orders of magnitude and switched to an ON state, Fig. 4, similar to that reported in [17]. After switching to the ON state at the highest temperature shown, the impedance was measured under bias with decreasing temperature. The air-processed sample maintained the ON state with almost zero activation energy down to room temperature (a) but the N_2-processed sample showed more complex behaviour (b). Its activation energy increased gradually on cooling and almost recovered its initial value, although the sample had much higher conductivity than the initial conductivity without dc bias.

The results in Fig. 4 show that both the number of charge carriers, n and their mobility, μ, which are related to the conductivity by:

$$\sigma = n\, e\, \mu \tag{5}$$

where e is the charge on an electron, are important parameters in controlling the conductivity profiles. The air-processed sample is a hopping conductor in the OFF state (a) with activation energy 0.62(1) eV, but a zero activation energy, delocalised conductor in the ON state. Its ON state conductivity,~ 10^{-2} Scm^{-1}, is about seven orders of magnitude less than that usually attributed to metallic conduction, which indicates a very small concentration of delocalised carriers in the BCF23 ON state. The N_2-processed sample shows a gradual change from delocalised to localised carriers on cooling under bias (b) although the concentration of mobile (electronic) carriers is still 5–6 orders of magnitude greater than in the original unbiased state of mixed *p*-type and oxide ion conduction.

In order to investigate possible flash luminescence during OFF-ON switching, an electrical field of 198 V/cm, with maximum current density, J_{max} of 61 mA/mm^2, was applied to the samples at 230 °C. The resistances were measured as a function of time and photo snap shots taken before, during and after application of the electrical field, Fig. 5. Both samples luminesced after switching their resistance to the ON state. It took longer,~ 8 mins, for the resistance and luminescence of the N_2-processed sample to switch, compared with the rapid switch in air. This effect is attributed in some way to its lower electronic conductivity in N_2 since the magnitude of the bulk ionic conductivity should be largely unaffected by the small differences in oxygen vacancy concentration and associated oxide ion conductivity in the two processing atmospheres. The luminescence of both samples subsequently faded after longer times in the ON state.

Further investigations were carried out in order to probe the effect of temperature, pO_2 and electrode polarity on the flash event. Samples were observed to luminesce over a wide range of temperatures from 200 to 915 ℃, Fig 6 and S4. At all temperatures, the flash event started at the top electrode and moved towards the bottom electrode (i.e. from the negative to the positive electrode). Below 200 ℃, no flash was seen at 198 V/cm with J_{max}=1200 mA (not shown). Above 200 ℃, luminescence appeared at 200 V/cm only if $J_{max} \geq 1000$ mA (~ 50 mA/mm^2), Fig S4. With increase in temperature, the luminescence intensity declined above 915 °C, and almost disappeared at 945 ℃, Fig. 6b. On subsequently decreasing the temperature, the luminescence recovered and its intensity increased (c).

The effect of *dc* bias, pO_2 and time on the flash event at 870 ℃ are shown in Fig. 7. Initial results to illustrate the effect of a bias are shown in (a) in which there was no luminescence before application and after removal of the electrical field in air, but luminescence with 198 V/cm bias. To show the effect of pO_2, application of 198 V/cm in N_2 (b), caused luminescence initially for less than 1 min which then started to decay until it had almost vanished after 4 min. On changing the atmosphere from N_2 to air without removing the field (b), the luminescence returned within 2 min but disappeared again on switching back to N_2. These combined results show that both pO_2 and the magnitude and

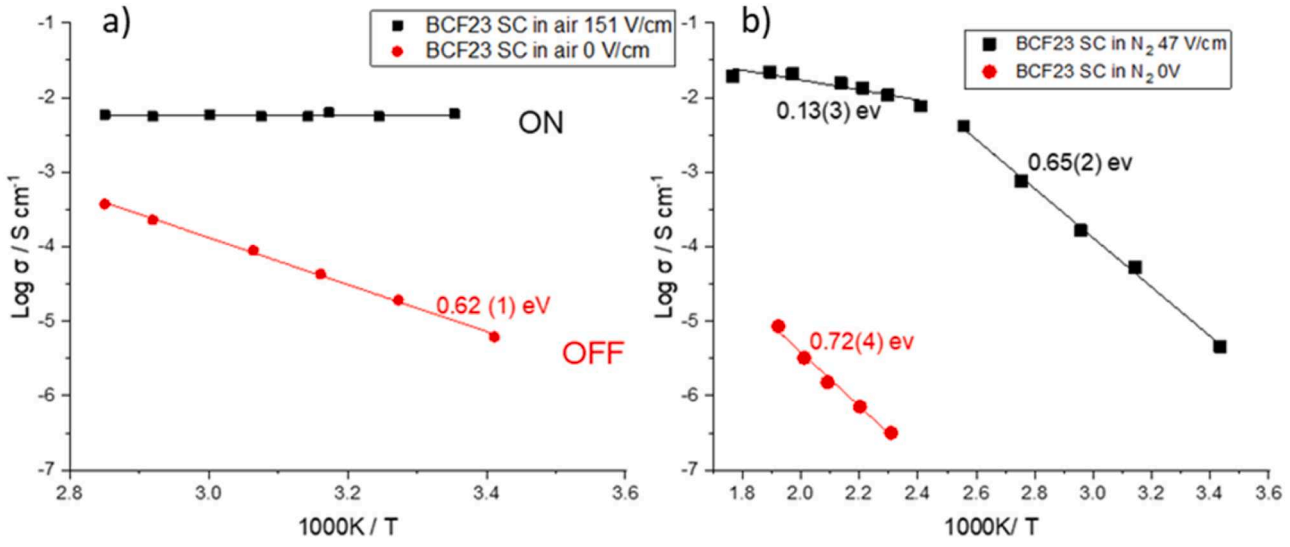

Fig. 4. Arrhenius conductivity plots of (a) air and (b) N_2-processed BCF23 on heating in the absence of applied bias (red) and on cooling with a *dc* bias (black).

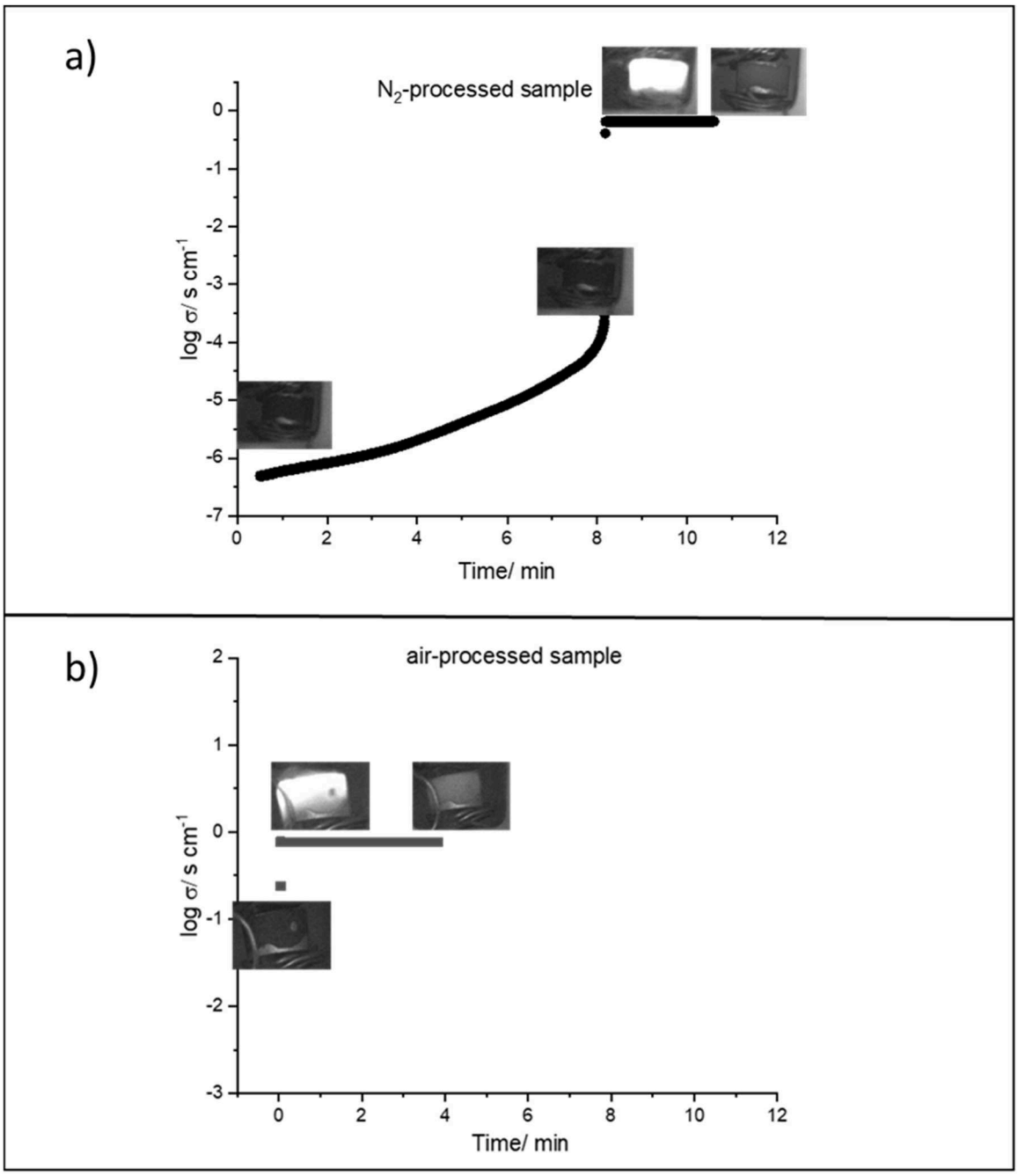

Fig. 5. The effect of application of 198 V/cm on the conductivities of (a) N_2-processed and (b) air-processed samples at 230 °C as a function of time, with inclusion of snap shots of the samples before and during the field application.

nature of the electronic conductivity play important roles in the flash mechanism.

4. Discussion

In the absence of an applied voltage, both YSH and BCF are oxide ion conductors associated with the oxygen vacancies, V_o, that are generated by the acceptor doping mechanisms:

$$Y_2O_3 = 2Y'_{Hf} + 3O_o^x + V_o^{\cdot\cdot} \quad (6)$$

$$2CaO = 2Ca'_{Bi} + V_O^{\cdot\cdot} + O_O^x \quad (7)$$

In both cases, the materials subsequently pick up O_2 from an oxygen-rich atmosphere which dissociates, oxygen atoms enter the oxygen vacancies and electron holes are created by redox reaction between these incoming oxygen molecules/atoms and adjacent lattice oxide ions, Eq. (1). The holes are responsible for *p*-type conductivity and therefore, an observed increase in conductivity with increasing pO_2 is evidence that the electronic conduction mechanism is *p*-type, in addition to any pre-existing oxide ion conductivity. The holes are located on either oxygen or Fe in BCF but must be located on oxygen in YSH because all the cations present are already in their highest oxidation states. In the absence of an applied voltage, both BCF and YSH show modest increases in *p*-type conductivity on switching the atmosphere from nitrogen to air during impedance measurements. A similar, but additional conductivity increase is observed with an applied field at lower temperatures and this is attributed to hole injection at the anode; the holes arise from ionisation of O^{2-} ions [17,18,20,21].

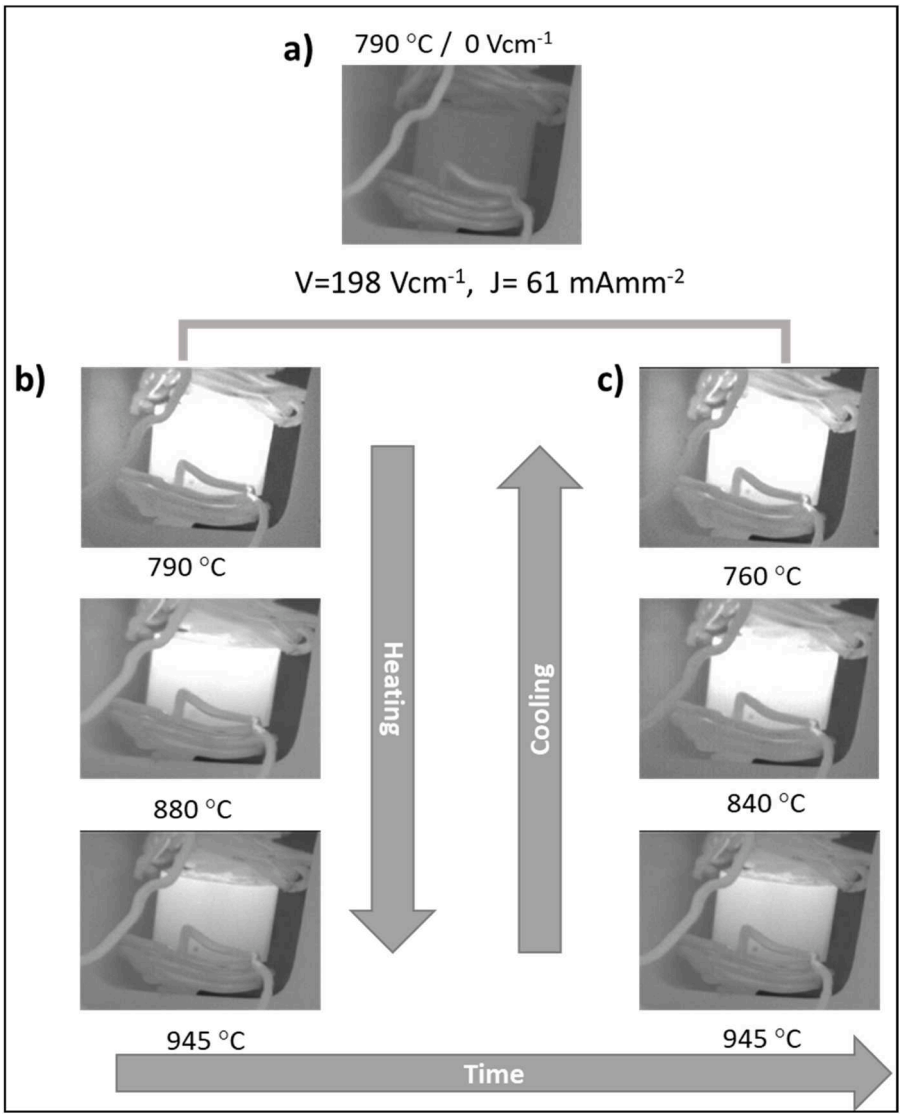

Fig. 6. The effect of temperature on the flash event: a) Photo of BCF23 pellet attached to the Pt wires of the jig and placed in the furnace at 790 °C before applying the electric field. Snap shots of the sample after applying 198 V/cm at different temperatures on heating (b) and on cooling (c).

Oxygen transport number measurements of YSH gave a value of 0.86 at 600 °C for $x = 0.15$ (YSH15) which increased to unity with temperature and decreased with increasing yttrium concentration at 800 °C [20]. Transport number measurements on Ca-doped BCF have not been made or reported but impedance measurements show that BCF23 is primarily a *p*-type conductor in air although it also has a high level of oxide ion conductivity as shown by impedance measurements in N_2 [22].

Application of a bias voltage to YSH15 and BCF23 at higher temperatures causes switching to an ON state and a change in electronic conduction mechanism. Since the ON state conductivity for both samples is higher in N_2 than in air, electrons are generated by means of O_2 loss, Eq. (2). At some point during the OFF-ON transition, and in the subsequent ON state, the bulk electronic conductivity of both BCF and YSH switches from modest *p*-type to a much higher *n*-type conductivity. Application of the bias voltage is critical to maintaining the ON state during subsequent cooling since without the bias, both materials return rapidly to the OFF state.

The flash luminescence that is observed with both materials coincides with the OFF-ON conductivity transition and is also triggered by changes of pO_2 in the surrounding atmosphere. Similar luminescence events and dramatic changes in conductivity have been observed in many materials during the flash sintering process. At the beginning, flash was attributed to solely black body radiation arising from Joule heating produced by the electrical current in addition to heating provided by the furnace. Later studies attributed the flash phenomenon to various causes, such as the formation of F-centre defects in Al_2O_3 [23] and gaseous discharge at ceramic interparticles in 3YSZ [24]. Analyses of the optical emission spectra suggested that the luminescence is due hole-electron recombination [25,26]. Muccillo et al. analysed the luminescence spectra during flash sintering of 8YSZ and Sm_2O_3-doped CeO_2 [27] and attributed flash luminescence mainly to Joule heating and emission solely to black body radiation. However, their results were not conclusive and they did not exclude the possibility of electron-hole recombination. One difficulty in interpreting the emission spectra appears to have been in separating the emissions from different possible sources such as furnace elements and other sources of heating. The mechanism(s) responsible for the luminescence is therefore, still an open question.

The luminescence observed here must be electroluminescent in character since (i) there are no significant changes with temperature simply as a consequence of luminescence caused by changing pO_2, (ii) temperature measurements recorded by a thermocouple in close proximity to the sample showed a maximum increase in temperature of < 10

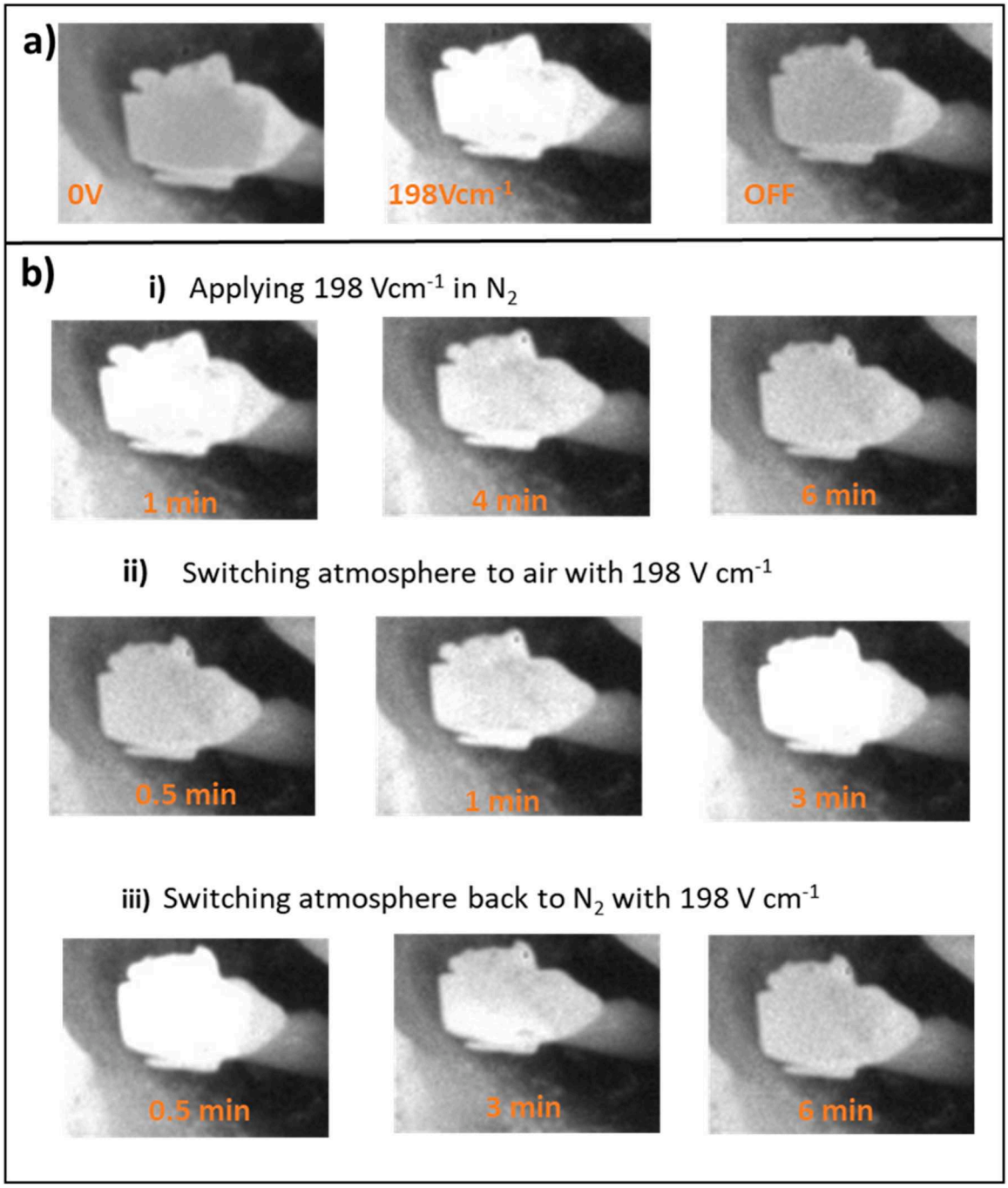

Fig. 7. (a) The effect of 198 Vcm^{-1} bias on the flash event at 870 °C in BCF23 showing the sample before, during and after removal of the bias, b) snap shots in different atmospheres on continuous application of 198 V/cm, (i) in N_2, (ii) in air and (iii) in N_2.

°C at the OFF-ON transition and (iii) the luminescence disappeared at highest temperature in BCF23, all of which rule out the occurrence of thermoluminescence under these conditions. The observed electroluminescence appears to be associated with charge carrier recombination, therefore, in particular at *pn* junctions. The various snapshots taken show that, on achieving the ON state, luminescence commences at the cathode and extends towards the anode. It is therefore linked to creation of *n*-type carriers that arise from O_2 loss, Eq. (2) which are injected at the cathode.

Prior to the OFF-ON transition, the electronic conductivity in both YSH15 and BCF23 is *p*-type and the conductivity can be increased by an applied field with hole injection at the anode. At the temperature of the OFF-ON transition, a dramatic increase in *n*-type electronic conductivity occurs which is associated with electron injection at the cathode. Hence a combination of electron injection at the cathode and hole injection at the anode leads to the creation of internal *pn* junctions whose formation / disappearance may be followed through the snapshots. In order to maintain the luminescence, a continual supply of both electrons and holes to the *pn* junctions is required. Particularly noteworthy is the gradual loss in luminescence with increasing temperature over the range 790–945 °C which is subsequently regained on cooling, Fig. 6. This reflects the natural tendency of many materials to lose oxygen at higher temperatures which is reversibly regained on cooling. Hence, in the conducting ON state, gas-solid equilibria are critical to the appearance of luminescence and to its OFF-ON switching by the spontaneous formation and disappearance of internal *pn* junctions.

The results reported here and in our earlier publications on resistive switching are related to those in a series of publications by Chen et al. [28-31] on reduction and *dc* degradation of yttria stabilised zirconia, YSZ, Gd-doped ceria and $SrTiO_3$ ceramics. The nature of their experimental studies were rather different to ours and showed microstructural differences between near-cathode and near-anode regions which were associated with differences in oxygen potential across the sample subjected to a *dc* bias. They also observed that 8YSZ loses oxygen above a critical voltage, becomes metallic on the cathode side, turning the sample black followed by thermal runaway flash [30]. Further work is required to better understand the mechanisms of flash sintering and especially the vast amounts of mass transfer that must occur; what we show here is that, by careful control of experimental conditions – temperature, pO_2, *dc* bias – it is possible to separate and characterise resistive switching and luminescence phenomena.

5. Conclusions

1) Flash electroluminescence is reported in two materials, fluorite-structured yttria-stabilised hafnia and Ca-doped bismuth ferrite perovskite, in which the previously-reported OFF-ON resistive switching is shown to be accompanied by OFF-ON luminescence.
2) Both materials are mixed oxide ion conducting and *p*-type in air. Their level of *p*-type conductivity depends on pO_2 and is controlled by the uptake, dissociation and ionisation of oxygen from the atmosphere.
3) Reversible OFF-ON resistive switching occurs under the influence of a *dc* bias which, at low fields causes hole injection at the anode and at higher fields, leads to oxygen evolution and electron injection at the cathode.
4) Flash luminescence involves electron - hole recombination at *pn* junctions that are activated primarily by hole injection at the anode.
5) The observed luminescence is electro- rather than thermo- in origin since the relatively low fields involved do not give a significant amount of Joule heating.
6) There appears to be a close link between the OFF-ON resistive switching and luminescence observed here and the widely-observed phenomenon of flash sintering, although additional mechanism(s) must be observed in the sintering which requires more severe conditions of applied bias and temperature.

CRediT authorship contribution statement

Fawaz Almutairi: Conceptualization, Investigation, Methodology. **Meshari Alotaibi:** Conceptualization, Investigation, Methodology. **Anthony R West:** Supervision, Writing – original draft, Writing – review & editing.

Declaration of competing interest

The authors declare that they have no known competing financial interests or personal relationships that could have appeared to influence the work reported in this paper.

Acknowledgment

Fawaz Almutairi thanks Imam Mohammad Ibn Saud Islamic University for a studentship.

Meshari Alotaibi acknowledges the Deanship of Scientific Research, Taif University for funding this work.

Supplementary materials

Supplementary material associated with this article can be found, in the online version, at doi:10.1016/j.actamat.2024.120003.

References

[1] C.E. Dancer, Flash sintering of ceramic materials, Mater. Res. Express 3 (10) (2016) 102001.
[2] M. Yu, S. Grasso, R. Mckinnon, T. Saunders, M.J. Reece, Review of flash sintering: materials, mechanisms and modelling, Adv. Appl. Ceram 116 (1) (2017) 24–60.
[3] M. Cologna, A.L. Prette, R. Raj, Flash-sintering of cubic yttria-stabilized zirconia at 750 °C for possible use in SOFC manufacturing, J. Am. Ceram. Soc. 94 (2) (2011) 316–319.
[4] R. Raj, A. Kulkarni, J.-M. Lebrun, S. Jha, Flash sintering: a new frontier in defect physics and materials science, MRS Bull 46 (2021) 36–43.
[5] B. Yoon, V. Avila, I.R. Lavagnini, J.V. Campos, L.M. Jesus, Reactive flash sintering of ceramics: a review, Adv. Eng. Mater. 25 (5) (2023) 2200731.
[6] F. Walz, The Verwey transition-a topical review, J. Phys.: Condens. Matter 14 (12) (2002) R285.
[7] J.P. Wright, J.P. Attfield, P.G. Radaelli, Charge ordered structure of magnetite Fe 3 O 4 below the Verwey transition, Phys. Rev. B 66 (21) (2002) 214422.
[8] J. García, G. Subías, The Verwey transition—A new perspective, J. Phys.: Condens. Matter 16 (7) (2004) R145.
[9] H.-T. Kim, B.-G. Chae, D.-H. Youn, S.-L. Maeng, G. Kim, K.-Y. Kang, Y.-S. Lim, Mechanism and observation of Mott transition in VO2-based two-and three-terminal devices, New J. Phys. 6 (1) (2004) 52.
[10] M. Imada, A. Fujimori, Y. Tokura, Metal-insulator transitions, Rev. Mod. Phys. 70 (4) (1998) 1039.
[11] N. Mott, Metal-Insulator Transitions, CRC Press, 2004.
[12] N.F. Mott, Metal-insulator transition, Rev. Mod. Phys. 40 (4) (1968) 677.
[13] Y. Wang, K.-M. Kang, M. Kim, H.-S. Lee, R. Waser, D. Wouters, R. Dittmann, J. J. Yang, H.-H. Park, Mott-transition-based RRAM, Mater. Today 28 (2019) 63–80.
[14] J.S. Lee, S. Lee, T.W. Noh, Resistive switching phenomena: a review of statistical physics approaches, Appl. Phys. Rev 2 (3) (2015).
[15] D.S. Jeong, R. Thomas, R.S. Katiyar, J.F. Scott, H. Kohlstedt, A. Petraru, C. S. Hwang, Emerging memories: resistive switching mechanisms and current status, Rep. Prog. Phys. 75 (7) (2012) 076502.
[16] D. Kumar, R. Aluguri, U. Chand, T.Y. Tseng, Metal oxide resistive switching memory: materials, properties and switching mechanisms, Ceram. Int. 43 (2017) S547–S556.
[17] N. Maso, H. Beltran, M. Prades, E. Cordoncillo, A.R. West, Field-enhanced bulk conductivity and resistive-switching in Ca-doped BiFeO3 ceramics, Phys. Chem. Chem. Phys. 16 (36) (2014) 19408–19416.
[18] M. Alotaibi, F. Almutairi, A.R. West, Resistive-switching in yttria-stabilized hafnia ceramics, J. Am. Ceram. Soc. 106 (2) (2022) 822–828.
[19] M. Biesuz, L. Pinter, T. Saunders, M. Reece, J. Binner, V.M. Sglavo, S. Grasso, Investigation of electrochemical, optical and thermal effects during flash sintering of 8YSZ, Materials (Basel) 11 (7) (2018) 1214.
[20] M. Alotaibi, L. Li, A.R. West, Electrical properties of yttria-stabilised hafnia ceramics, Phys. Chem. Chem. Phys. 23 (45) (2021) 25951–25960.
[21] A.R. West, Redox-active oxygen in oxides: emergent applications, including field-induced resistive switching, flash luminescence, p–n junctions and high capacity battery cathodes, J. Mater. Chem. A 11 (2023) 12681–12694.
[22] N. Masó, A.R. West, Electrical Properties of Ca-Doped BiFeO3 Ceramics: from p-Type Semiconduction to Oxide-Ion Conduction, Chem. Mater. 24 (11) (2012) 2127–2132.
[23] M. Biesuz, V.M. Sglavo, Current-induced abnormal and oriented grain growth in corundum upon flash sintering, Scripta Mater 150 (2018) 82–86.
[24] R. Muccillo, E. Muccillo, Light emission during electric field-assisted sintering of electroceramics, J. Eur. Ceram. Soc. 35 (5) (2015) 1653–1656.
[25] R. Raj, D.E. Wolf, C.N. Yamada, S.K. Jha, J.M. Lebrun, On the confluence of ultrafast high-temperature sintering and flash sintering phenomena, J. Am. Ceram. Soc. 106 (7) (2023) 3983–3998.
[26] S.K. Jha, K. Terauds, J.-M. Lebrun, R. Raj, Beyond flash sintering in 3 mol% yttria stabilized zirconia, J. Ceram. Soc. Jpn. 124 (4) (2016) 283–288.
[27] R. Muccillo, J.C.C. Diaz, E.N. Muccillo, Analysis of the Luminescent Emission during Flash Sintering of 8YSZ and 20SDC Ceramics, Ceramics 7 (1) (2024) 329–341.
[28] Y. Dong, H. Wang, I.W. Chen, Electrical and hydrogen reduction enhances kinetics in doped zirconia and ceria: I. grain growth study, J. Am. Ceram. Soc. 100 (3) (2017) 876–886.
[29] Y. Dong, I.W. Chen, Electrical and hydrogen reduction enhances kinetics in doped zirconia and ceria: II. Mapping electrode polarization and vacancy condensation in YSZ, J. Am. Ceram. Soc. 101 (3) (2018) 1058–1073.
[30] A. Alvarez, Y. Dong, I.W. Chen, DC electrical degradation of YSZ: voltage-controlled electrical metallization of a fast ion conducting insulator, J. Am. Ceram. Soc. 103 (5) (2020) 3178–3193.
[31] A. Alvarez, I.W. Chen, DC resistance degradation of SrTiO3: the role of virtual-cathode needles and oxygen bubbles, J. Am. Ceram. Soc. 105 (1) (2022) 362–383.